Pergamon
www.elsevier.com/locate/asr

Adv. Space Res. Vol. 27, No. 4, pp. 717–726, 2001

Printed in Great Britain
0273-1177/01 $20.00 + 0.00
PII: S0273-1177(01)00112-0

MODELS FOR GALACTIC COSMIC-RAY PROPAGATION

A.W. Strong[1] and I.V. Moskalenko[2*†]

[1] *Max-Planck-Institut für extraterrestrische Physik, Postfach 1312, 85741 Garching, Germany*
[2] *NASA/Goddard Space Flight Center, Code 660, Greenbelt, MD 20771, USA*

ABSTRACT

A new numerical model of particle propagation in the Galaxy has been developed, which allows the study of cosmic-ray and gamma-ray production and propagation in 2D or 3D, including a full reaction network. This is a further development of the code which has been used for studies of cosmic ray reacceleration, Galactic halo size, antiprotons and positrons in cosmic rays, the interpretation of diffuse continuum gamma rays, and dark matter. In this paper we illustrate recent results focussing on B/C, sub-Fe/Fe, ACE radioactive isotope data, source abundances and antiprotons. From the radioactive nuclei we derive a range of 3–7 kpc for the height of the cosmic-ray halo.

INTRODUCTION

In recent years, new and accurate data have become available in cosmic-ray (CR) astrophysics, and much progress in understanding the origin and propagation of CR can be made, but this requires a systematic and self-consistent approach. With this motivation we have developed a numerical propagation code which aims to reproduce observational data of many kinds related to CR, such as direct measurements of nuclei, antiprotons, positrons and electrons, gamma rays and synchrotron radiation.

In the first version, the model was cylindrically symmetric and was written in fortran-90. This version has proven that the original goal, a "realistic standard model" of CR production and propagation, is possible to achieve. It has been used for studies of CR reacceleration, halo size, production and propagation of positrons and antiprotons, dark matter annihilation, and the interpretation of diffuse continuum gamma rays. Many aspects, however, cannot be addressed in such a model, e.g. the stochastic nature of the CR sources in space and time which is important for high-energy electrons with short cooling times, and local inhomogeneities in the gas density which can affect radioactive secondary ratios in CR.

The experience gained from the original version allowed us to design a new version of the model, entirely rewritten in C++, which is much more flexible, which incorporates essential improvements over the older model, and in which a 3-dimensional spatial grid can be employed. In addition it is now possible to solve the full nuclear reaction network on the spatially resolved grid. We keep however an option which allows us to switch to the older cylindrically symmetrical ("2D") model since this is still a sufficient approximation for nuclei in the absence of spatial fluctuations and is much faster to compute than the full 3D case.

The code can thus serve as a complete substitute for the conventional "leaky-box" or "weighted-slab" propagation models usually employed, with many associated advantages such as the correct treatment of radioactive nuclei, realistic gas and source distributions etc. The present work illustrates the use of the new 2D code to interpret B/C, sub-Fe/Fe, new radioactive isotopic ratio data from ACE, source abundances and antiprotons.

*NRC Senior Research Associate
†on leave from Institute of Nuclear Physics, M.V.Lomonosov Moscow State University, Moscow 119899, Russia

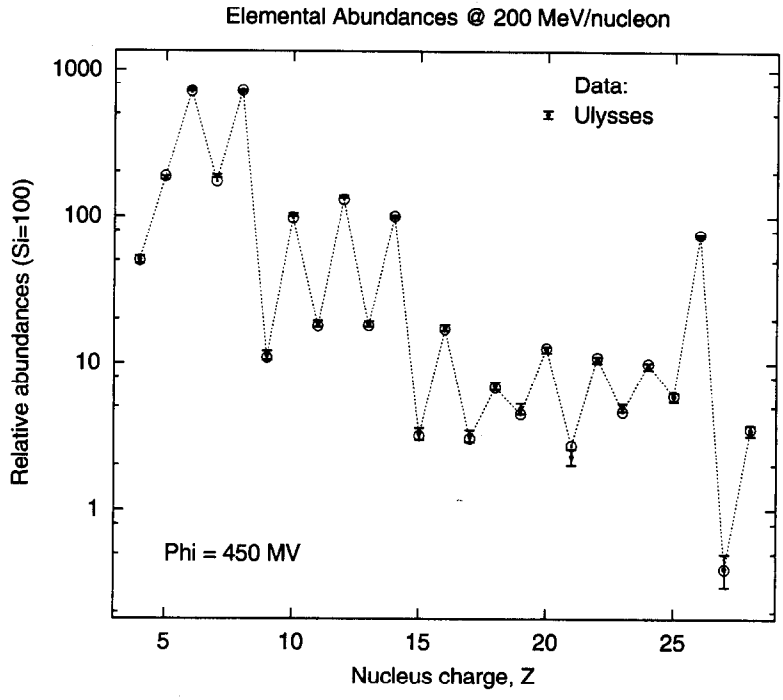

Fig. 1. Relative CR propagated elemental abundances as calculated in our model at 200 MeV/nucleon in the heliosphere – circles. Modulation potential $\Phi = 450$ MV. Data: Duvernois and Thayer (1996) – vertical bars.

MODELS

The GALPROP models have been described in full detail elsewhere (Strong and Moskalenko 1998); here we just summarize briefly their basic features. The results obtained with the original version of GALPROP have been discussed in a recent review (Strong and Moskalenko 1999).

The 2D models have cylindrical symmetry in the Galaxy, and the basic coordinates are (R, z, p) where R is Galactocentric radius, z is the distance from the Galactic plane and p is the total particle momentum. The propagation region is bounded by $R = R_h$, $z = \pm z_h$ beyond which free escape is assumed. We take $R_h = 30$ kpc. For a given z_h the diffusion coefficient as a function of momentum and the reacceleration parameters is determined by the energy-dependence of the B/C ratio. Reacceleration provides a natural mechanism to reproduce the B/C ratio without an ad-hoc form for the diffusion coefficient. The spatial diffusion coefficient is taken as $\beta D_0(\rho/\rho_0)^\delta$, assuming independence of position, where ρ is rigidity. We use values of δ near but not necessarily equal to the Kolmogorov value of $\delta = 1/3$. For the case of reacceleration the momentum-space diffusion coefficient D_{pp} is related to the spatial coefficient (e.g. Seo and Ptuskin 1994). The reacceleration is parameterized by v_A^2/w where v_A is the Alfvén speed and w the ratio of wave energy density to magnetic field energy density (Seo and Ptuskin 1994). The injection spectrum of nuclei is assumed to be a power law in momentum, $dq(p)/dp \propto p^{-\gamma}$ for the injected particle density, if necessary with a break.

The interstellar hydrogen distribution uses HI and CO surveys and information on the ionized component; the Helium fraction of the gas is taken as 0.11 by number. Energy losses of nuclei by ionization and Coulomb interactions are included.

The distribution of CR sources is chosen to reproduce the CR distribution determined by analysis of EGRET gamma-ray data (Strong and Mattox 1996). The source distribution adopted was described in Strong and Moskalenko (1998). It adequately reproduces the observed gamma-ray based gradient, while being significantly flatter than the observed distribution of supernova remnants.

The primary source abundances are adjusted to give as good agreement as possible with the observed abundances after propagation (Figure 1), for a given set of cross-sections. The heliospheric modulation is

taken into account using the force-field approximation.

In the new version, apart from the option of a full 3D treatment, we have updated the cross-section code to include latest measurements and energy dependent fitting functions. The nuclear reaction network is built using the Nuclear Data Sheets. The isotopic cross section database consists of more than 2000 points collected from sources published in 1969–1999. This includes a critical re-evaluation of some data and cross checks. The isotopic cross sections for B/C were calculated using the authors' fits to major beryllium and boron production cross sections C,N,O $\rightarrow$ Be,B. Other cross sections are calculated using the Webber et al. (1990)[3] and/or Silberberg and Tsao[4] phenomenological approximations renormalized to the data where it exists. In this paper we use our fits combined with the Webber et al. approximation renormalized to available data.

The reaction network is solved starting at the heaviest nuclei (i.e. ^{64}Ni), solving the propagation equation, computing all the resulting secondary source functions, and proceeding to the nuclei with $A - 1$. The procedure is repeated down to $A = 1$. In this way all secondary, tertiary etc. reactions are automatically accounted for. To be completely accurate for all isotopes, e.g. for some rare cases of $\beta^{\pm}$-decay, the whole loop is repeated twice.

PROPAGATION OF COSMIC RAYS

From the point of view of isotope ratios, the main advance here is our employment of the full reaction network. For this purpose the 2D model is sufficient.

Figure 2 shows the predicted local interstellar (LIS) and modulated B/C ratio compared with observations; the reacceleration reproduces the peak quite well. The new ACE data (Davis et al. 2000) confirm the presence of the peak and give an improved basis for fitting the reacceleration. Note that the modulation potential estimated for the ACE data by Davis et al. is $\Phi = 350$ MV; our calculations made with $\Phi = 400 - 500$ MV agree with the ACE data, and we adopt 450 MV in what follows. The model we consider has a diffusion coefficient index $\delta = 0.36$ and injection spectrum index $\gamma = 2.35$. We find that a value of $v_A/w^{1/2} = 31$ km s^{-1} gives the best match. A "Kolmogorov" model with $\delta = 1/3$ ($v_A/w^{1/2} = 24$ km s^{-1}) gives less satisfactory agreement with the high-energy data.

Figure 3 shows (Sc+Ti+V)/Fe for the same model. The agreement is quite good given that the model was not fitted to this ratio; this ratio favours $\delta = 0.36$, and less satisfactorily matched by $\delta = 1/3$.

As in previous work we study the halo size z_h using ^{10}Be and other radioactive isotopes. For each z_h the model is adjusted to fit B/C and then the radioactive nuclei are compared with data. Figure 4 shows ^{10}Be/^{9}Be; notice that the rapid falloff in the ratio at low energies, which is caused by the variation in the ^{12}C$\rightarrow^{10}$Be cross-section, is critical, and makes this ratio rather sensitive to the modulation. Derivation of z_h from ^{10}Be/^{9}Be is discussed below. Observations at higher energies, where modulation is smaller, will greatly help in this regard.

For the heavier radioactive nuclei the procedure is first to adjust the source abundances at the appropriate energy to agree with the relevant observed stable nuclei ratios and then derive the fluxes of the radioactive isotopes. In this way the uncertainty in the denominator of the ratio is reduced. Figures 5–7 show ^{26}Al/^{27}Al, ^{36}Cl/Cl and ^{54}Mn/Mn. The ACE data points imply halo sizes of a few kpc. Some uncertainty arises from the error bars on the elemental abundance measurements from Ulysses, to which we tune our propagated abundances. The dominant uncertainty comes however from the cross-sections and the modulation, while the experimental values for the ratios measured by ACE are rather accurate.

We now try to take into account the cross section and abundance errors. The calculated abundances of the four radioactive isotopes at 200 MeV/nucleon (100 MeV/nucleon for Be) and $\Phi = 450$ MV are shown in Table 1 for different halo sizes. The ratios in the Table are calculated using Ulysses elemental abundances (DuVernois and Thayer 1996) normalized to silicon (Si=100): Al = 18.5$\pm$0.8, Cl = 3.2$\pm$0.3, Mn = 5.9$\pm$0.4. This removes some uncertainty in the denominator for these ratios. The first error bar was obtained from the elemental abundance error, the second error bar is larger and obtained assuming 20% error in the production cross sections of ^{36}Cl and ^{54}Mn, and 35% error for ^{26}Al. When deriving the halo size these translate into a

[3]Code `WNEWTR.FOR` of 1993 as posted at `http://spdsch.phys.lsu.edu/SPDSCH_Pages/Software_Pages/Cross_Section_Calcs/WebberKishSchrier.html`

[4]Code `YIELDX_011000.FOR` of 2000 as posted at `http://spdsch.phys.lsu.edu/SPDSCH_Pages/Software_Pages/Cross_Section_Calcs/SilberburgTsao.html`

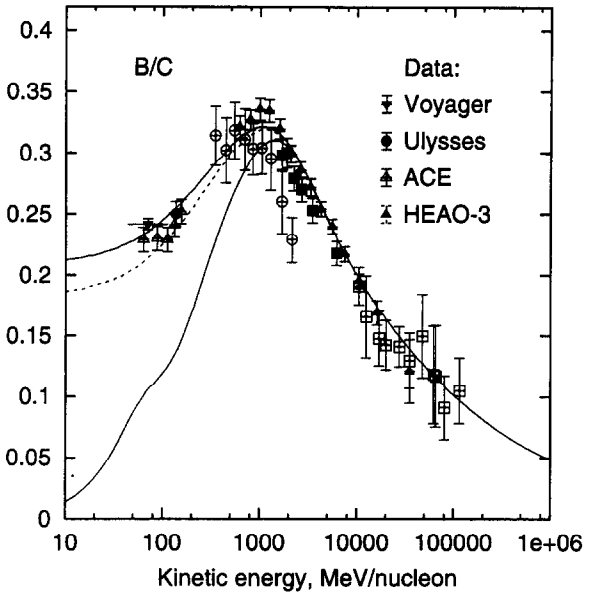

Fig. 2. B/C ratio calculated for $z_h = 4$ kpc. Lower curve LIS, upper modulated. Model with $(\delta, \gamma) = (0.36, 2.35)$: solid curve – $\Phi = 500$ MV, dotted curve – 400 MV. Data below 200 MeV/nucleon: ACE – Davis et al. (2000), Ulysses – DuVernois et al. (1996), Voyager – Lukasiak et al. (1999); high energy data: HEAO-3 – Engelmann et al. (1990), for other references see Stephens and Streitmatter (1998).

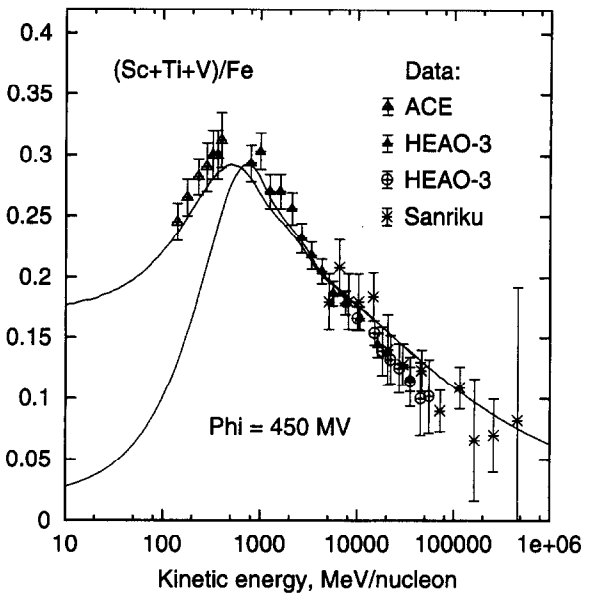

Fig. 3. SubFe/Fe ratio calculated for $z_h = 4$ kpc. Lower curve LIS, upper modulated. Model with $(\delta, \gamma) = (0.36, 2.35)$. Data: ACE – Davis et al. (2000), HEAO-3 – Binns et al. (1988) and Engelmann et al. (1990), Sanriku experiment – Hareyama et al. (1999). We used HEAO-3 data only below 45 GeV because of absence of vanadium measurements above this energy.

wide range of halo sizes since the difference between calculated abundances for 4 and 6 kpc, and 6 and 10 kpc halos is only about 10%. Assuming the errors in Table 1 are independent, the total error estimate may thus be 30% or even larger, making the halo size estimates all consistent with a lower limit of ~ 3 kpc.

The case of Be is slightly different. All Be isotopes are purely secondary, so that we cannot tune their abundances by varying the source abundance. While the elemental abundance agrees well with Ulysses measurements, the relative isotopic fraction of ^{7}Be is 10% less and ^{9}Be is 15% more than measured (Connell 1998): ^{7}Be = 0.561, ^{9}Be = 0.393, ^{10}Be = 0.046. The Be isotope production cross sections, we believe, are more accurate than those for most other nuclei since we use fits to the major production channels. We therefore take the largest deviation (15%) as an estimate of ^{10}Be production cross section error. The ratio in Table 1 is obtained using the measured fraction of ^{9}Be. The corrected value then gives the range $z_h = 1.5 - 6.0$ kpc.

Figure 8 summarizes the halo size constraints based on the four radioactive isotopes considered using ACE data (Yanasak et al. 2000). These have been calculated by requiring consistency of the calculated ratio with the ACE data taking into account the error bars on both prediction and data. The conclusion to be drawn from all radioactive nuclei is that we require $z_h = 3 - 7$ kpc, i.e. a large halo, at least within the context of the models considered here. This is consistent with our previous result $z_h = 4 - 10$ kpc (Strong and Moskalenko 1998) based on Ulysses data (Connell 1998), and now the ACE data lead to a more robust estmate. It is also consistent with other results, e.g., Webber and Soutoul (1998) found $z_h = 2 - 4$ kpc from HEAO-3, and Ptuskin and Soutoul (1998) give 4.9^{+4}_{-2} kpc.

Table 2 lists propagated and source isotopic abundances at 200 MeV/nucleon ($\Phi = 450$ MV) for $z_h = 4$ kpc. All abundances are normalized to ^{16}O. The Source/Solar System elemental abundance ratios are shown in Figure 9, where the solar system abundances have been taken from Anders and Grevesse (1989). Our

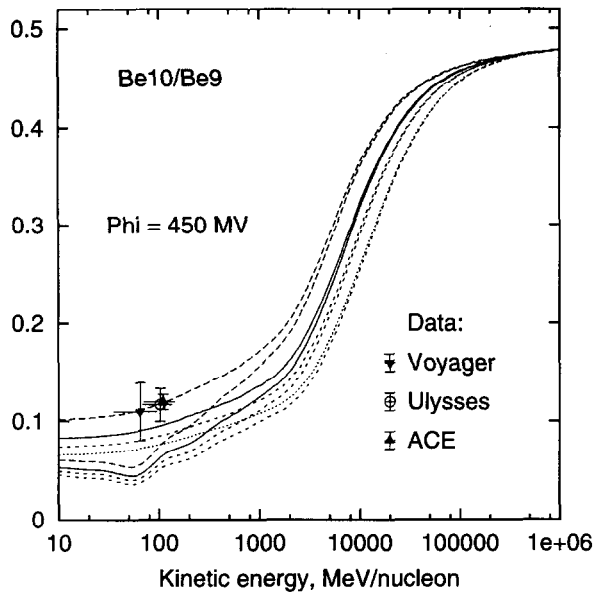

Fig. 4. ^{10}Be/^{9}Be ratio calculated for $z_h = 2, 4, 6, 10$ kpc (top to bottom). Lower curves LIS, upper modulated. Data: ACE – Yanasak et al. (2000), Ulysses – Connell (1998), Voyager – Lukasiak et al. (1999).

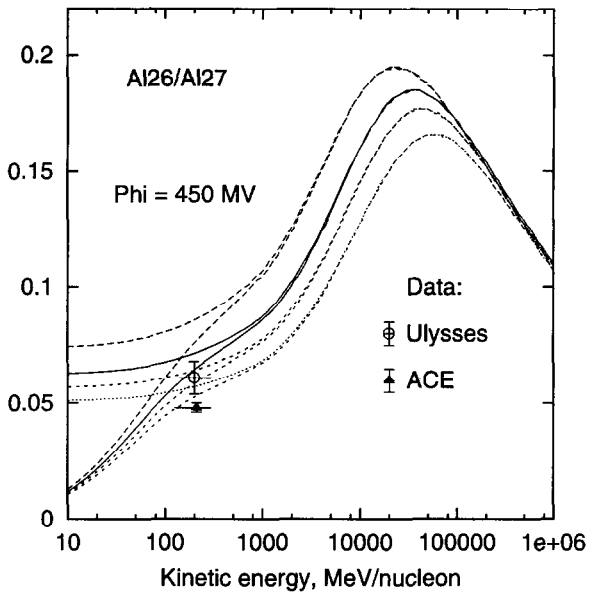

Fig. 5. ^{26}Al/^{27}Al ratio calculated for $z_h = 2, 4, 6, 10$ kpc (top to bottom). Lower curves LIS, upper modulated. Data: ACE – Yanasak et al. (2000), Ulysses – Simpson and Connell (1998).

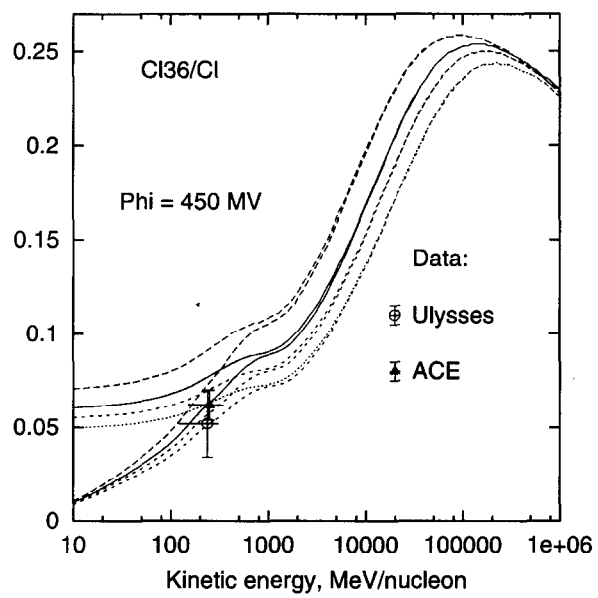

Fig. 6. ^{36}Cl/Cl ratio calculated for $z_h = 2, 4, 6, 10$ kpc (top to bottom). Lower curves LIS, upper modulated. Data: ACE – Yanasak et al. (2000), Ulysses – Connell et al. (1998).

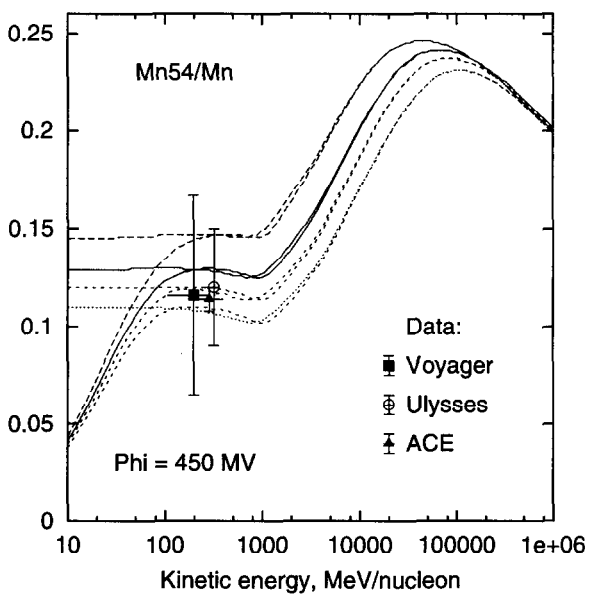

Fig. 7. ^{54}Mn/Mn ratio calculated for $z_h = 2, 4, 6, 10$ kpc (top to bottom). Lower curves LIS, upper modulated. Data: ACE – Yanasak et al. (2000), Ulysses – DuVernois (1997), Voyager – Lukasiak et al. (1997).

Table 1. Radioactive isotopic abundances (Si=100)*.

z_h	^{10}Be	^{10}Be/^{9}Be†, 10^{-1}	^{26}Al	^{26}Al/^{27}Al, 10^{-2}	^{36}Cl	^{36}Cl/Cl, 10^{-2}	^{54}Mn	^{54}Mn/Mn, 10^{-1}
2 kpc	2.27	$1.33\ ^{+0.20}_{-0.17}$	1.44	$8.44\ ^{+0.42\ +3.30}_{-0.38\ -2.32}$	0.268	$8.38\ ^{+0.87\ +1.68}_{-0.72\ -1.40}$	0.900	$1.53\ ^{+0.11\ +0.31}_{-0.10\ -0.25}$
4 kpc	1.84	$1.09\ ^{+0.16}_{-0.14}$	1.20	$6.91\ ^{+0.31\ +2.65}_{-0.33\ -1.88}$	0.225	$7.04\ ^{+0.73\ +1.41}_{-0.60\ -1.17}$	0.769	$1.30\ ^{+0.10\ +0.26}_{-0.08\ -0.22}$
6 kpc	1.62	$0.97\ ^{+0.15}_{-0.13}$	1.07	$6.16\ ^{+0.30\ +2.34}_{-0.27\ -1.67}$	0.203	$6.35\ ^{+0.66\ +1.27}_{-0.54\ -1.06}$	0.697	$1.18\ ^{+0.09\ +0.24}_{-0.08\ -0.20}$
10 kpc	1.41	$0.87\ ^{+0.13}_{-0.11}$	0.952	$5.42\ ^{+0.26\ +2.04}_{-0.24\ -1.46}$	0.179	$5.60\ ^{+0.58\ +1.12}_{-0.48\ -0.93}$	0.624	$1.06\ ^{+0.08\ +0.21}_{-0.07\ -0.18}$
ACE data‡		1.20 ± 0.08		4.8 ± 0.2		6.2 ± 0.8		1.14 ± 0.06

*The error bars derived (i) using the elemental abundance error, (ii) assuming 20% error in the production cross sections of ^{36}Cl and ^{54}Mn, and 35% error for ^{26}Al.

†Error bars derived assuming 15% error in ^{10}Be production cross section.

‡Yanasak et al. (2000).

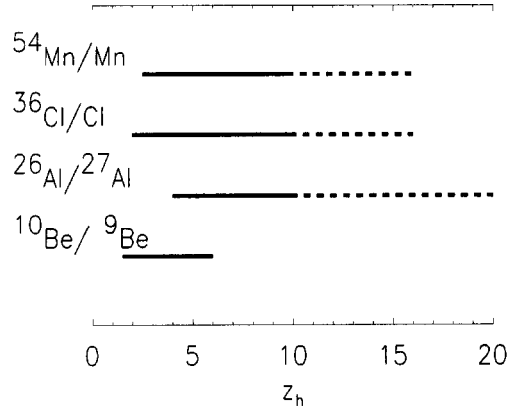

Fig. 8. Halo size limits as derived from the abundances of the four radioactive isotopes (Table 1) and ACE data. The ranges reflect errors in ratio measurements, source abundances and production cross-sections. Dashed lines indicate uncertain upper limits. The shaded area indicates the range consistent with all ratios.

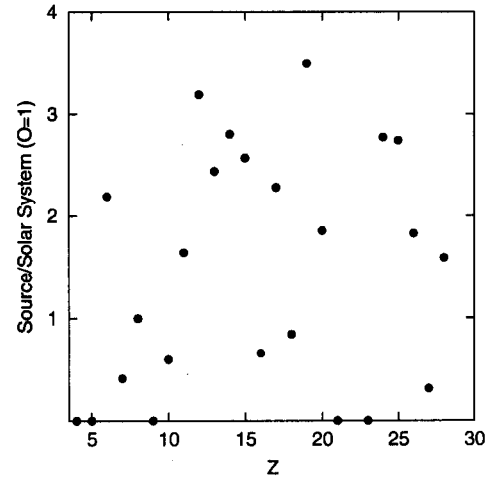

Fig. 9. Elemental source/solar system abundance ratio, ([O] = 1). Solar system abundances are from Anders and Grevesse (1989).

derived source abundance of Ti relative to Fe seems to be high, while the propagated abundances (Figures 1, 3) are satisfactory. This source abundance is however very sensitive to the production cross sections. Note also that since we use consistent propagation parameters for the entire range of nuclei rather than adjusting for separate groups as is often done, this reduces our freedom to adjust the source abundances. Source abundances of largely secondary nuclei ^{33}S, ^{41}Ca, ^{50}Cr, ^{58}Fe, ^{59}Co, and isotopes of Cl, Ti and Ni are small and also essentially depend on the production cross sections, and the error here thus may be as large as 100%. The typical overall error of our source abundances for other nuclei can be estimated as about 20% based on conservative estimates of the cross section errors.

The process of electron K-capture from the ISM is not currently included so that K-capture isotopes such as ^{49}V, ^{51}Cr, ^{55}Fe, and ^{57}Co are over-estimated by 20–50%, while their daughter nuclei ^{49}Ti, ^{51}V, ^{54}Cr, ^{55}Mn are under-estimated by 20–100%. Inclusion of the process of electron K-capture will improve their isotopic abundances and will allow study of the CR acceleration time scale. Since production and decay of K-capture isotopes and radioactive isotopes depends critically on the matter density distribution, our next

Table 2. Propagated and source isotopic abundances (^{16}O=100).

	Z, A	Prop. abund.	Source abund.		Z, A	Propagated abundances	Source abundances		Z, A	Propagated abundances	Source abundances
Be	4, 7	3.62	–	S	16,32	1.73	2.64	Ti*	22,50	3.853×10^{-2}	4.901×10^{-2}
	4, 9	3.21	–		16,33*	0.305	5.717×10^{-2}	V	23,49†	0.368	–
	4,10	0.337	–		16,34	0.387	0.172		23,50	0.224	–
B	5,10	7.46	–		16,36	2.251×10^{-2}	–		23,51‡	7.123×10^{-2}	–
	5,11	19.2	–	Cl*	17,35	0.252	2.450×10^{-2}	Cr	24,50*	0.235	5.990×10^{-2}
C	6,12	94.2	69.4		17,36	3.289×10^{-2}	–		24,51†	0.377	–
	6,13	7.66	0.681		17,37	0.153	8.712×10^{-2}		24,52	0.609	0.286
N	7,14	12.0	4.76	Ar	18,36	0.399	0.681		24,53	0.160	0.127
	7,15	12.6	–		18,37	0.148	–		24,54*‡	4.416×10^{-2}	3.812×10^{-2}
O	8,16	100.	100.		18,38	0.364	0.136	Mn	25,53	0.390	0.106
	8,17	1.21	–		18,40	6.236×10^{-2}	–		25,54	0.110	–
	8,18	1.37	–	K	19,39	0.321	0.136		25,55‡	0.351	0.272
F	9,19	1.55	–		19,40	0.143	–	Fe	26,54	0.894	1.96
Ne	10,20	8.24	8.44		19,41	0.178	–		26,55†	0.514	0.329
	10,21	1.52	–	Ca	20,40	0.578	1.17		26,56	9.02	21.1
	10,22	4.21	2.53		20,41*	0.126	2.723×10^{-2}		26,57	0.349	0.784
Na	11,23	2.56	0.572		20,42	0.357	–		26,58*	2.582×10^{-2}	3.839×10^{-2}
Mg	12,24	13.3	17.0		20,43	0.374	–	Co	27,56	1.374×10^{-2}	–
	12,25	2.66	2.20		20,44	0.375	–		27,57†	3.250×10^{-2}	–
	12,26	2.67	2.74		20,46	3.037×10^{-3}	–		27,59*	1.024×10^{-2}	1.089×10^{-2}
Al	13,26	0.172	–	Sc	21,45	0.392	–	Ni*	28,56	4.479×10^{-4}	–
	13,27	2.40	1.47	Ti*	22,44	1.264×10^{-2}	–		28,58	0.321	0.833
Si	14,28	12.1	18.5		22,46	0.375	–		28,59	1.826×10^{-2}	2.205×10^{-2}
	14,29	1.48	1.63		22,47	0.478	6.806×10^{-2}		28,60	0.144	0.359
	14,30	0.727	0.545		22,48	0.588	0.272		28,61	6.345×10^{-3}	9.529×10^{-3}
P	15,31	0.458	0.218		22,49‡	7.615×10^{-2}	–		28,62	1.831×10^{-2}	4.411×10^{-2}

*Source abundances error can be as large as 100%.
†Propagated abundance over-estimated since K-capture.
‡Propagated abundance under-estimated as K-capture daughter nucleus.

goal is therefore to include this process in the model. More details will be given in a forthcoming paper.

The relative isotopic fraction within an element for the purely secondary nucleus B, and secondary isotopes of Ca, Ti, V, and Co are in good agreement with measurements (B: Lukasiak et al. 1999). The same is true for abundances of pure secondary F and Sc. As already mentioned, ^{7}Be is slightly under-predicted and ^{9}Be is over-predicted compared to measurements (Connell 1998, Lukasiak et al. 1999).

The current elemental abundances were tuned to be consistent with low energy measurements by Ulysses (DuVernois and Thayer 1996). The isotopic composition of Cl has been tuned to Ulysses data (Connell et al. 1998), Ca, Ti, V, Cr, Co to Voyager data (Lukasiak et al. 1997a,b), S, Mn, Ni to Ulysses (Connell and Simpson 1997, DuVernois 1997, Thayer 1997) and Voyager data (Lukasiak et al. 1997a,b, Webber et al. 1997, Lukasiak et al. 1999), C, N, O, Ne, Mg to Voyager (Webber et al. 1996, Webber et al. 1997) and CRRES data (Duvernois et al. 1996), and Si and Fe using Voyager (Lukasiak et al. 1997a, Webber et al. 1997), ALICE (Hesse et al. 1996), CRRES data (Duvernois et al. 1996), and Ulysses data (Connell and Simpson 1997).

This is however a preliminary result in the sense that there is still a problem with tuning elemental and isotopic abundances over the whole energy range. There is some disagreement with the elemental abundances at higher energies by HEAO-3 (Engelmann et al. 1990), which is not surprising considering that the measurements show somewhat different spectral indices for different isotopes while we use a single power-law injection index. On the other hand, the isotopic composition measurements are carried out at energies which are strongly affected by solar modulation. Employing a model which is better than a simple force-field approximation will be vital for further analysis. Our neglect of K-capture is another reason why these results are preliminary and intended to illustrate the method rather than provide a basis for interpretation.

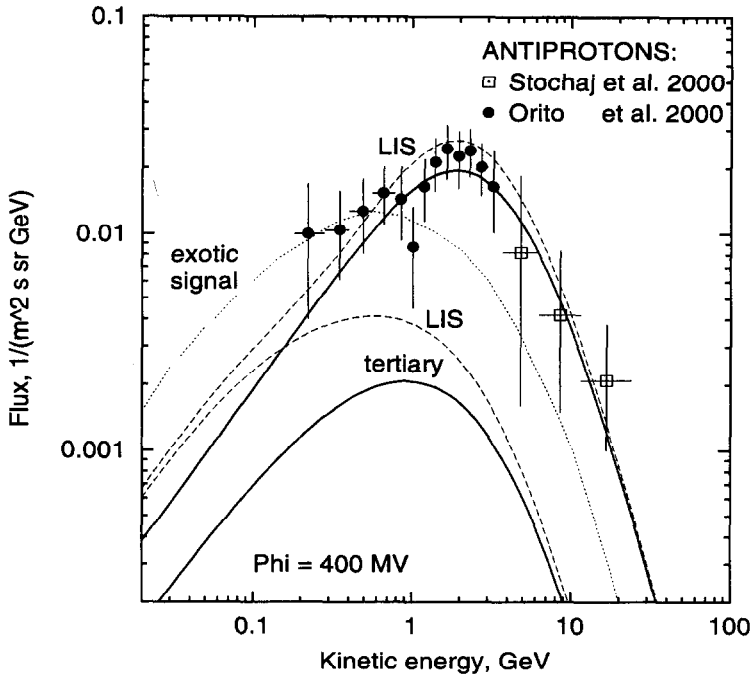

Fig. 10. Calculated antiproton LIS and modulated spectrum with data: BESS – Orito et al. (2000), MASS91 – Stochaj et al. (2000). The top curves are the total background. The "tertiary" components (LIS and modulated) are shown separately. Also shown is an example exotic signal Bergström et al. (1999) extended to lower energies.

SECONDARY ANTIPROTONS

Secondary positrons and antiprotons in Galactic CR and some part of the diffuse Galactic gamma rays are produced in collisions of CR particles with interstellar matter[5]. Because they are secondary, they reflect the *large-scale* nucleon spectrum independent of local irregularities in the primaries and thus provide an essential check on propagation models and also on the interpretation of diffuse gamma-ray emission (Strong et al. 2000). These are an important diagnostic for models of CR propagation and provide information complementary to that provided by secondary nuclei. However, unlike secondary nuclei, antiprotons and positrons reflect primarily the propagation history of the protons, the main CR component.

Secondary antiprotons have been computed in the same model as for the nuclei. The halo size has been set to 4 kpc; the exact value is unimportant for antiproton calculations provided the propagation parameters are tuned to match B/C ratio. The adopted nucleon injection spectrum, after propagation, matches the local one. We calculate antiproton production and propagation using the basic formalism described in Moskalenko et al. (1998). To this we have added antiproton annihilation and treated inelastically scattered antiprotons as a separate "tertiary" component. The antiproton production by nuclei with $Z \geq 2$ is calculated in two ways: employing scaling factors as described in Moskalenko et al. (1998), and using effective factors given by Simon et al. (1998), who make use of the DTUNUC code, and which appears to be more accurate than simple scaling. (The use of the Simon et al. factors is consistent since their adopted proton spectrum resembles our spectrum above the antiproton production threshold.) The effect on the antiproton flux at low energies is however small, and the two approaches differ by about 15%.

The results are shown in Figure 10 (Moskalenko et al. 2001). The upper curves are the local interstellar flux and the lower are modulated. The two lowest curves show separately the contribution of "tertiary" antiprotons, which is the dominant component at low energies. There still remains an excess for the lowest energy points at the 1σ level which may indicate an additional component.

[5]Contributions from possible nearby source(s), black hole evaporation, and WIMP annihilation into positrons and antiprotons are also discussed.

CONCLUSIONS

It is now possible to make a spatially resolved treatment of a full reaction network with a realistic model of the Galaxy and CR propagation. Reacceleration with a slighly larger index for the diffusion coefficient than the Kolmogorov law fits B/C, sub-Fe/Fe and CR antiprotons quite well over the whole energy range. The halo size indicated by the four radioactive isotope ratio measured by ACE is in the range 3 – 7 kpc, but the dispersion between the isotopes is large presumably due to cross-section inaccuracies. In fact the CR measurements have now become relatively more accurate than the cross section measurements, so that the latter become a factor restricting further progress.

To remove uncertainty connected with elemental abundances errors and denominator production cross sections, we propose in future to use ratios like radioactive secondary/major primary, namely ^{26}Al/^{28}Si, ^{36}Cl/^{56}Fe, and ^{54}Mn/^{56}Fe instead of widely used ^{26}Al/^{27}Al, ^{36}Cl/Cl, and ^{54}Mn/Mn. The ratio ^{54}Mn/^{56}Fe is probably the best candidate because there are only very minor contributions from other nuclei. In the case of Be, the ratio ^{10}Be/^{12}C is probably better than ^{10}Be/^{9}Be. Finally, the accurate measurement of all isotopic abundances by one experiment, e.g. ACE, will help greatly to constrain the problem.

ACKNOWLEDGEMENTS

The authors thank F. Jones, V. Ptuskin, and A. Lukasiak for helpful discussions, and S.A. Stephens and R.A. Streitmatter for providing the database of B/C measurements. I. Moskalenko acknowledges support from NAS/NRC Senior Research Associateship Program.

REFERENCES

Anders, E., and N. Grevesse, Abundances of the elements – meteoritic and solar, *Geochim. Cosmochim. Acta* **53**, 197-214, 1989.

Bergström, L., J. Edsjö, and P. Ullio, Cosmic antiprotons as a probe for supersymmetric dark matter?, *ApJ* **526**, 215-235, 1999.

Binns, W. R., T. L. Garrard, M. H. Israel, M. D. Jones, M. P. Kamionkowski, et al., Cosmic-ray energy spectra between 10 and several hundred GeV per atomic mass unit for elements from ^{18}Ar to ^{28}Ni: results from HEAO 3, *ApJ* **324**, 1106-1117, 1988.

Connell, J. J., Galactic cosmic-ray confinement time: Ulysses high energy telescope measurements of the secondary radionuclide ^{10}Be, *ApJ* **501**, L59-L62, 1998.

Connell, J. J., and J. A. Simpson, Isotopic abundances of Fe and Ni in Galactic cosmic-ray sources, *ApJ* **475**, L61-L64, 1997.

Connell, J. J., M. A. Duvernois, and J. A. Simpson, The cosmic-ray radioactive nuclide ^{36}Cl and its propagation in the Galaxy, *ApJ* **509**, L97-L100, 1998.

Davis, A. J., R. A. Mewaldt, W. R. Binns, E. R. Christian, A. C. Cummings, et al., On the low energy decrease in Galactic cosmic ray *Proc. ACE-2000 Symp., eds. Mewaldt, R. A., J. R. Jokipii, M. A. Lee, E. Möbius, and T. H. Zurbuchen (NY: AIP), AIP Conf. Proc.* **528**, 421-424, 2000.

DuVernois, M. A., Galactic cosmic-ray manganese: Ulysses high energy telescope results, *ApJ* **481**, 241-252, 1997.

DuVernois, M. A., and M. R. Thayer, The elemental composition of the Galactic cosmic-ray source: Ulysses high-energy telescope results, *ApJ* **465**, 982-984, 1996.

DuVernois, M. A., J. A. Simpson, and M. R. Thayer, Interstellar propagation of cosmic rays: analysis of the Ulysses primary and secondary elemental abundances, *A&A* **316**, 555-563, 1996.

DuVernois, M. A., M. Garcia-Munoz, K. R. Pyle, J. A. Simpson, and M. R. Thayer, The isotopic composition of galactic cosmic-ray elements from carbon to silicon: the Combined Release and Radiation Effects Satellite investigation, *ApJ* **466**, 457-472, 1996.

Engelmann, J. J., P. Ferrando, A. Soutoul, P. Goret, and E. Juliusson, Charge composition and energy spectra of cosmic-ray nuclei for elements from Be to Ni – Results from HEAO-3-C2, *A&A* **233**, 96-111, 1990.

Hareyama, M., M. Ichimura, E. Kamioka, T. Kobayashi, S. Kuramata, et al., Sub-Fe/Fe ratio obtained by Sanriku balloon experiment, *26th ICRC (Salt Lake City)* **3**, 105-108, 1999.

Hesse, A., B. S. Acharya, U. Heinbach, W. Heinrich, M. Henkel, et al., Isotopic composition of silicon and iron in the galactic cosmic radiation, *A&A* **314**, 785-794, 1996.

Lukasiak, A., F. B. McDonald, and W. R. Webber, Voyager measurements of the mass composition of cosmic-ray Ca through Fe nuclei, *ApJ* **488**, 454-461, 1997a.

Lukasiak, A., F. B. McDonald, W. R. Webber, and P. Ferrando, Voyager measurements of the isotopic composition of Fe, Co and Ni nuclei – implications for the nucleosynthesis and the acceleration of cosmic rays, *Adv. Space Res.* **19**, 747-750, 1997b.

Lukasiak, A., F. B. McDonald, and W. R. Webber, Voyager measurements of the charge and isotopic composition of cosmic ray Li, Be and B nuclei and implications for their production in the Galaxy, *26th ICRC (Salt Lake City)* **3**, 41-45, 1999.

Moskalenko, I. V., A. W. Strong, and O. Reimer, Diffuse Galactic gamma rays, cosmic-ray nucleons and antiprotons, *A&A* **338**, L75-L78, 1998.

Moskalenko, I. V., E. R. Christian, A. A. Moiseev, J. F. Ormes, and A. W. Strong, Antiprotons below 200 MeV in the interstellar medium: perspectives for observing exotic matter signatures, *Proc. COSPAR Coll. "The Outer Heliosphere: The Next Frontiers"*, in press, 2001.

Ptuskin, V. S., and A. Soutoul, Decaying cosmic ray nuclei in the local interstellar medium, *A&A* **337**, 859-865, 1998.

Orito, S., T. Maeno, H. Matsunaga, K. Abe, K. Anraku, et al., Precision measurements of cosmic-ray antiproton spectrum, *Phys. Rev. Lett.* **84**, 1078-1081, 2000.

Seo, E. S., and V. S. Ptuskin, Stochastic reacceleration of cosmic rays in the interstellar medium, *ApJ* **431**, 705-714, 1994.

Simon, M., A. Molnar, and S. Roesler, A new calculation of the interstellar secondary cosmic-ray antiprotons, *ApJ* **499**, 250-257, 1998.

Simpson, J. A., and J. J. Connell, Cosmic-ray ^{26}Al and its decay in the Galaxy, *ApJ* **497**, L85-L88, 1998.

Stephens, S. A., and R. A. Streitmatter, Cosmic-ray propagation in the Galaxy: Techniques and the mean matter traversal, *ApJ* **505**, 266-277, 1998.

Stochaj, S. J., R. L. Golden, M. Hof, C. Pfeifer, W. Menn, et al., The flux of cosmic ray antiprotons from 3.7 to 24 GeV, *ApJ*, in press, 2000.

Strong, A. W., and J. R. Mattox, Gradient model analysis of EGRET diffuse Galactic gamma-ray emission, *A&A* **308**, L21-L24, 1996.

Strong, A. W., and I. V. Moskalenko, Propagation of cosmic-ray nucleons in the Galaxy, *ApJ* **509**, 212-228, 1998.

Strong, A. W., and I. V. Moskalenko, Galactic cosmic rays and gamma rays: a unified approach, in Topics in Cosmic Ray Astrophysics (vol.230 in Horizons in World Physics), ed. M. A. DuVernois, Nova Science Publishers, New York, NY, pp.81-103, 1999.

Strong, A. W., I. V. Moskalenko, and O. Reimer, Diffuse continuum gamma rays from the Galaxy, *ApJ* **537**, 763-784, 2000. Erratum: *ApJ* **541**, 1109, 2000.

Thayer, M. R., An investigation into sulfur isotopes in the galactic cosmic rays, *ApJ* **482**, 792-795, 1997.

Webber, W. R., J. C. Kish, and D. A. Schrier, Formula for calculating partial cross sections for nuclear reactions of nuclei with $E \geq 200$ MeV/nucleon in hydrogen targets, *Phys. Rev. C* **41**, 566-571, 1990.

Webber, W. R., A. Lukasiak, F. B. McDonald, and P. Ferrando, New high-statistical–high-resolution measurements of the cosmic-ray CNO isotopes from a 17 year study using the Voyager 1 and 2 spacecraft, *ApJ* **457**, 435-439, 1996.

Webber, W. R., A. Lukasiak, and F. B. McDonald, Voyager measurements of the mass composition of cosmic ray Ne, Mg, Si, and S nuclei, *ApJ* **476**, 766-770, 1997.

Webber, W. R., A. Soutoul, A study of the surviving fraction of the cosmic-ray radioactive decay isotopes measured on HEAO-3, *ApJ* **506**, 335-340, 1998.

Yanasak, N. E., W. R. Binns, E. R. Christian, A. C. Cummings, A. J. Davis, et al., Abundances of the cosmic ray β-decay secondaries and implications for cosmic ray transport, *Proc. ACE-2000 Symp., eds. Mewaldt, R. A., J. R. Jokipii, M. A. Lee, E. Möbius, and T. H. Zurbuchen (NY: AIP), AIP Conf. Proc.* **528**, 402-405, 2000.